Improved Doppler Picture Velocimetry and new Automated Processing

Friedrich Seiler[1], Alexander Pichler[1], Raphael Pfaff[2], Alfred George[1], Julio Srulijes[1]

1: French-German Research Institute of Saint-Louis (ISL), 68301 Saint-Louis, France, julio.srulijes@isl.eu
2: Control Theory and Applications Centre, Coventry University, Coventry CV1 5FB, pfaffr@coventry.ac.uk

Abstract A unique technique, the Doppler Picture Velocimetry (DPV), for measuring and visualizing velocities especially in hypersonic gas flows is presented. By means of a Michelson interferometer (MI) the Doppler shifted light scattered by tracers is transformed into an image showing Fizeau fringes. The image fringe distribution provides information on the Doppler frequency shift that is related to the velocity of the particles crossing the light sheet plane. To overcome former DPV disadvantages, the optical set-up and the processing scheme were significantly improved. Two schemes for fringe processing are presented: 1) a semi-automated interactive processing software and 2) a new algorithm based on a technique using Fast Fourier Transformations (FFT) to examine the DPV images in the frequency domain. This last DPV algorithm now allows an automated calculation of the velocity profiles from the Doppler pictures without manual fringe tracing as had to be done in the past. Both methods are compared by means of Mach 6 flows around a wedge and a sphere inside the ISL shock tunnel STA. The flow is seeded with TiO_2 particles. These particles are illuminated by a laser light sheet perpendicular to the main flow direction. Light observation via the MI from the side informs on the vertically oriented velocity through the DPV images.

1. Introduction

1.1 History

Several laser-based techniques have been developed worldwide for measuring the flow velocity distribution in a light sheet, i.e. in a plane, crossing a gas flow. A well-known technique is Particle Image Velocimetry (PIV), which relies on the statistical analysis of geometrical particle displacements (Merzkirch 1990). The Doppler Global Velocimetry (DGV) analyses the Doppler frequency shift of light scattered by tracer particles by an amplitude light filter (Meyers 1992). The Doppler frequency can also be analysed by a special wide-field Michelson interferometer (MI) designed at ISL (Oertel et al. 1982). This method has been further developed by Seiler et al. (1987), and is known as Doppler Picture Velocimetry (DPV). Several disadvantages, concerning particularly the optical set-up of the MI, have already been improved as described in Seiler et al. (2002). The actual DPV-version (Seiler et al. 2004) uses two pictures, which are taken simultaneously: a Doppler picture showing the frequency shift of the light scattered by the moving tracer particles and a reference picture with no frequency shift. In the paper of Seiler et al. (2004), a simple and straightforward user manipulated DPV picture processing algorithm is described and applied for evaluating the velocity picture published. Two enhancements of this processing algorithm, a semi-automated and an automated one, are discussed in this paper. The semi-automated DPV picture analysis method developed by Pfaff et al. (2005) requires manual fringe tracing by the operator and is quite time consuming. For that reason, Pichler et al. (2007) developed a new automated DPV image processing software without need of fringe tracing. This processing scheme uses an FFT-algorithm (Fast Fourier Transformation) to examine the Doppler images in the frequency domain. Pfaff (2007) developed an alternative automated process based on the Least Square Estimators (LES) comprehensively described by Seiler et al. (2008a).

1.2 Aim of Work

This paper presents both, a semi-automated and a fully-automated processing software for the evaluation of the fringe images produced by the DPV-method. Although many software tools for PIV and DGV are available, the existing procedures are not suitable to process the DPV pictures taken with the optical MI set-up given in Fig. 1. The Doppler images are interferometric fringe images with a determined structure, in the present case a $\cos^2$-shaped system of fringes, which is distorted by mainly two sources of noise, i.e., the particle distribution and the digital camera used. While the particle distribution disturbs the light intensity distribution in the Doppler images, the camera introduces the so-called readout noise and the image sensor noise. The readout noise is caused in the conversion process from CCD registers to grey values in analogue to digital converters, amplifiers and charge to voltage converters. It is commonly assumed to be Gaussian white noise. Further noise sources are present in form of lenses, beam splitters and polarising screens in the optical set-up. These noise sources can be neglected due to their comparably small influence. The noise source can thus be assumed to be additive white noise with exception of the particle distribution noise, which is a low-frequency component.

2 The Doppler Picture Velocimetry technique

2.1 Michelson Interferometer

The DPV technique for the measurement of a velocity field in a gas flow is based on the observation of light reflected from tracer particles contained in the flow. The flow is illuminated with monochromatic coherent light and the resulting Doppler shift of the reflected light is visualized by use of a Michelson interferometer (MI). The interferometer makes it possible to measure the frequency shifts in the range of 10^{-5} of the original frequency for Mach 6 flows by transforming it into a fringe shift in the Fizeau fringe pattern, on which the MI is adjusted.

The DPV technique uses a unique MI, see Fig. 1, as described by Seiler et al. (2006). The laser light with frequency ν_L is divided into two parts by a splitter cube with a 30%-to-70% light intensity ratio. The 30% part is focused onto two dispersion plates in the reference plane Σ. Nowadays, the use of two plates compared with only one greatly reduces unwanted speckle noise in the reference image (Pichler et al. 2007). The 70%-part illuminates the flow plane Σ which crosses the gas flow as a light sheet. In order to visualize the velocity distribution in the flow plane Σ, TiO_2 tracer particles are seeded and the light scattered from these particles is focused into the specially designed MI, which is used here as a wide field interferometer. In the same way, the light coming from the dispersion plates, the so called reference light, is also directed into the MI as depicted in Fig. 1. The “reference” light bundle is coloured in blue and the “Doppler shifted” light bundle in yellow. The polarising beam splitter T1 perpendicularly polarizes both parts to each other. Entering the MI the “reference” light and the “Doppler shifted” light (tinted in green, blue and yellow), pass geometrically the same ways but are completely independent from each other.

The MI in Fig.1 consists of a beam splitter cube T2, the two mirrors M_1 and M_2 and the glass block G between M_2 and T. The scattered light coming from the object planes Σ, the tracer scattered light as well as the reference light, is divided by the second beam splitter T2 into two parts of equal intensity, which are focused on mirror M_1 (leg 1) and on mirror M_2 (leg 2). With the lenses used, the image of the planes Σ (dispersion plates and tracers) on M_1 and M_2 is transferred via the polarizing beam splitter T3 to the image planes Σ', forming the Doppler picture on the CCD1 camera and the reference picture on CCD2. The light passing the two interferometer legs 1 and 2 is able to form a two beam interference pattern in the image planes Σ'.

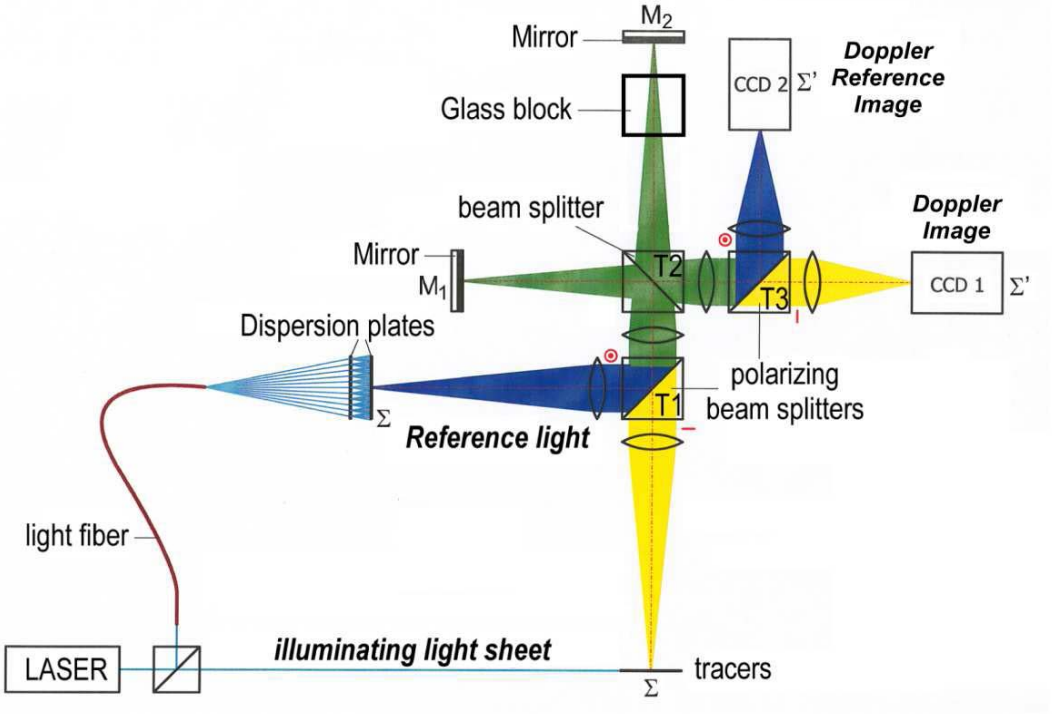

Fig. 1 Optical set-up of the Michelson interferometer

As a result of that interference the light intensity I at all image points P′ in Σ′, on the CCD1 as well as on the CCD2 camera chip, depends on the phase difference Δφ originated in the two legs as given in the following:

$$I = \hat{I} \cos^2 \frac{\Delta\varphi}{2} . \qquad (1)$$

The phase difference Δφ is a function of the optical path difference Δϕ, see Seiler et al. (2006):

$$\frac{\Delta\varphi}{2\pi} = \nu \frac{\Delta\phi}{c_0} . \qquad (2)$$

The optical path difference is defined as

$$\Delta\phi = 2n\left|\ell_2 - \ell_1\right| . \qquad (3)$$

By differentiating equation (2) with regard to dν, the result is:

$$d\left(\frac{\Delta\varphi}{2\pi}\right) = \frac{\Delta\phi}{\lambda_0}\frac{d\nu}{\nu} . \qquad (4)$$

The light scattered from the light sheet plane Σ is, in the case of moving tracer particles, Doppler shifted from frequency ν_R (R: laser reference) to ν_D. (D: detector, i.e. the MI). The frequency change of the scattered light, as seen by the MI,

$$d\nu = \nu_D - \nu_R , \qquad (5)$$

is transformed into a change d(Δφ), see equation (4), of the phase difference Δφ between the two legs of the Michelson interferometer.

The d(Δφ) change causes at each pixel of the CCD cameras variations

$$dI = -d(\Delta\varphi)\frac{\hat{I}}{2}\sin\Delta\varphi \qquad (6)$$

of the interference light intensity illuminating the CCD1 plane Σ′ compared with the initially adjusted light intensity distribution on CCD2. This dI-change ($dI = I_D - I_R$) informs on the d(Δφ)-shift and by relation (4) on the frequency shift dν, which is proportional to the tracer speed. The initially adjusted intensity distribution I_R and the Doppler shifted distribution I_D are represented by

- (I_R): the reference picture which is formed by the light coming from the dispersion plate and passing the MI not frequency shifted (blue coloured light path in Fig.1) and
- (I_D): the Doppler picture created by the light scattered by tracer particles crossing the light sheet (yellow coloured light path in Fig.1).

Both pictures, the reference and the Doppler picture, are taken simultaneously as described in Pichler et al. (2007), replacing the former DPV version (Seiler et al. 2002), in which both pictures could only be taken one after the other.

2.2 Adjustment

The MI is adjusted to interference fringes by turning the mirror M_1 by a very small angle β to produce a linear changing optical path difference Δϕ along M_1, see Fig. 1. The amount of fringes which appear in the image planes Σ′ depend on the turning angle β. As an example, fringe systems are depicted in Figs. 5, 10 and 11 for the DPV experiments performed with a wedge in a high-speed Mach-6-flow.

3 The shock tube as hypersonic wind tunnel

3.1 Shock tunnel STA

Nowadays the shock tubes at ISL are employed as hypersonic wind tunnels. The shock tube itself is divided into the high pressure driver tube and the low pressure driven tube, see Fig. 2. In the driver tube a preferably light driver gas is compressed up to 450 bars. At a determined driver-gas pressure the steel membrane dividing the high and low-pressure parts bursts. In this moment, a compression shock runs through the driven tube where nitrogen is contained under a pressure of up to 5 bar. At the same time an expansion wave runs in the opposite direction and is reflected from the left end of the driver tube. The compression shock propels the gas in the driven tube in front of the entry of the Laval nozzle where it is compressed and heated and where it remains for a short time almost stationary. The driven gas then expands through the Laval nozzle resulting in a quasi-stationary hypersonic flow into the measurement chamber. The resulting measurement time ranges from 1 up to 4 ms. Tests covered in this work were performed at Mach number 6 and at a static pressure of 8 ± 0.5 kPa and a temperature of about 220 K, resembling the conditions in the atmosphere at an altitude of 17.5 km. For this nozzle conditions a measurement time of about 2 ms is achieved.

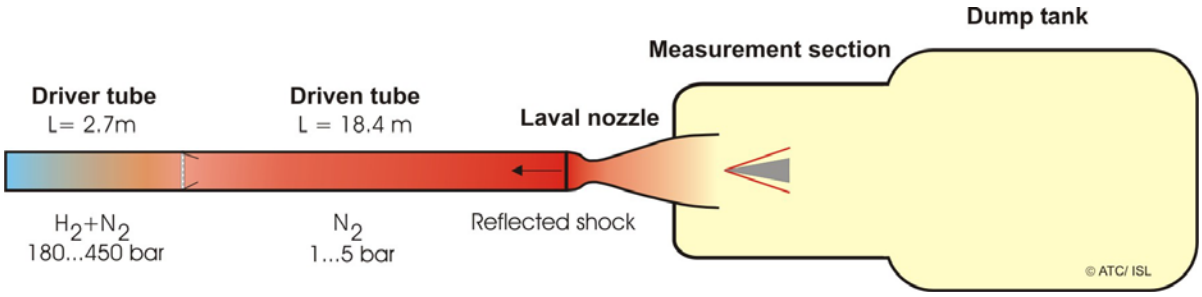

Fig. 2 Principle sketch of shock tunnel STA of ISL

3.2 Optical set-up

The Mach-6-nozzle used in shock-tunnel STA is mounted at the end of the driven tube and blows into the measurement section, mounted in front of the dump tank. Through windows at each side and one at the top, an optical access for flow illumination and flow observation is achieved. Fig. 3 shows the illuminating optics, a laser light sheet hitting the wedge from above, and the observation of the scattered light via the MI from the side. The light sheet is produced by a laser (vector $\vec{L}$ in Fig. 4) which illuminates a plane axially oriented in the middle of the wedge flow. The observation by means of the MI was done from the side in the direction of vector $\vec{R}$. The wedge flow is quasi two-dimensional, with flow vectors $\vec{u}$ (horizontal orientation) and $\vec{v}$ (vertical orientation, see Fig. 4). With this optical set-up, the projection of the velocity component $\vec{v}$ in the bisector of the angle formed by the illumination and observation directions is measured.

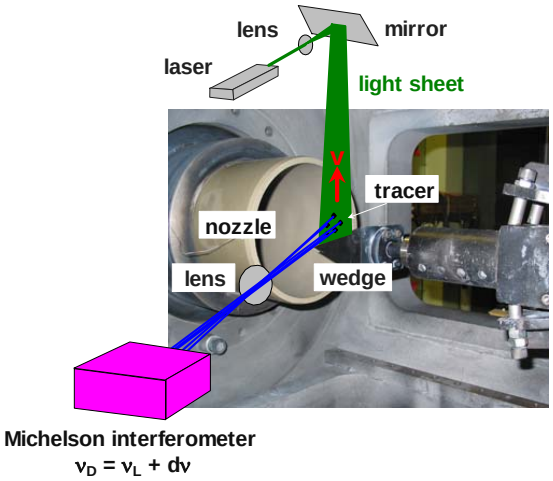

Fig. 3 DPV picture visualization

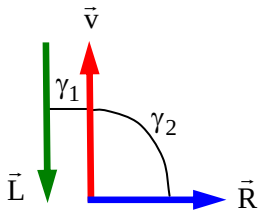

Fig. 4 Vectors $\vec{L}$, $\vec{R}$ and $\vec{v}$

4 Semi-automated algorithm

4.1 Processing tool

The picture processing tools are explained for the experiments done to measure the wedge flow velocity by DPV. The MI is adjusted to interference fringes by turning mirror M_1, see section 2.2. The fringe pattern over the wedge in the Mach-6-shock-tunnel flow is given in Fig. 5. A reference fringe pattern is taken simultaneously with the Doppler picture presented in Fig. 5. The Doppler

picture was taken at the shock tunnel flow conditions given in section 3.1. For illumination of the light sheet plane over the wedge flow, a continuously running Ar^+-laser was used. Its wavelength is 514.5 nm. The CCD-camera shutter was opened for 2 ms.

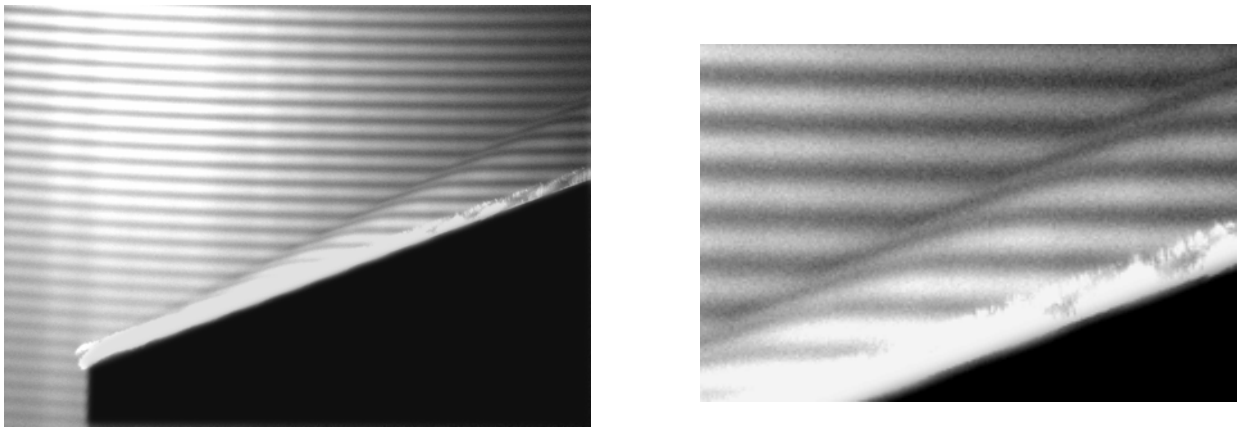

Fig. 5 Wedge flow Doppler picture in Σ'

The vertical velocity induced over the wedge surface causes a Doppler shift dν of the frequency ν_L of the light scattered by the tracer particles, here titanium dioxide (TiO_2), resulting in a light intensity change dI across the wedge shock wave, see section 2.1. This produces the fringe displacement in Fig. 5 showing the velocity jump across the bow wave attached to the tip of the wedge. On the right side of Fig. 5 an enlarged view of the DPV fringe shift is seen in detail.

An interactive working tool developed by Pfaff et al. (2005, 2007) processes the Doppler pictures using the Sun Microsystems "Java Advanced Imaging Bibliotheca" (2005). The drawings, especially the pseudo colour images, were prepared with the Matlab software and the Matlab Image Processing Toolbox (The MathWorks Inc. 2005). First, the reference picture and the Doppler picture are matched in size and rotation by using markers. In the second step, the distribution of the dark fringe lines with $I(x,y)=0$ is evaluated in the transformed images: first for the reference picture and then for the Doppler picture. There, the light intensity is specified by equation (1) and equals zero. The Doppler and the reference pictures are directly treated on the computer screen. By mouse click the user marks, point by point, the centre of the dark fringe lines. These points are linearly interpolated and stored in a $n \times m$ matrix, which size is similar to that of the CCD chip of the "Pixelfly QE" camera used, i.e., 1374 x 1024 pixels. The dark lines from the Doppler picture in Fig. 5 are shown in Fig. 6.

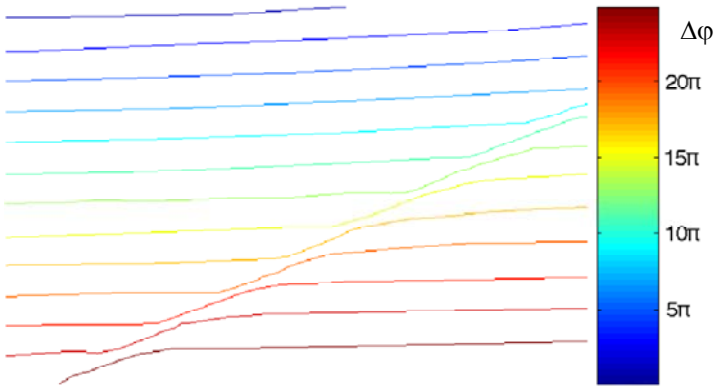

Fig. 6 Dark fringes, phase difference distribution

The fringe contours in Fig. 5 clearly show the shock wave influenced region over the wedge surface by a light intensity change dI which is seen in Fig. 6 as a shift of the processed dark fringes. It can be recognized that the shift of the fringe lines develops smoothly across the wedge shock wave due to the particle relaxation effect. The fringe shift in the shock influenced region over the wedge gives a measure of the shift of the phase difference $\Delta\varphi$. This is caused by the Doppler shift of the frequency $d\nu$ of the scattered light, see equation (4). From Fig. 6, a fringe shift of about one fringe, i.e., $\Delta\varphi \approx 2\pi$ can be estimated.

4.2 DPV velocity evaluation

Each dark line shown in Fig. 5 represents a line of constant phase difference $\Delta\varphi$. On this fringe pattern, the phase difference $\Delta\varphi$ change from line to line is described as follows:

$$\Delta\varphi(x,y) = (2k-1)\pi\,, \quad k = (...,-2,-1,0,1,2,...) \quad . \tag{7}$$

The dark-fringe-phase-difference distribution is shown in a pseudo colour scale on the right side in Fig. 6. In order to complete the $n \times m$ matrix points the following procedure is applied: the open spaces between the phase difference lines with $\Delta\varphi(x,y) = (2k-1)\pi$ are reconstructed orthogonally to the reference fringe system. Since equation (1) is valid between the dark lines, the fringes are linearly interpolated, yielding at the $n \times m$ mesh points the phase differences $\Delta\varphi_R$ for the reference picture and $\Delta\varphi_D$ for the Doppler picture. The phase pictures obtained are presented as pseudo colour distribution in Figs. 7a and 7b for both the Doppler and the reference pictures.

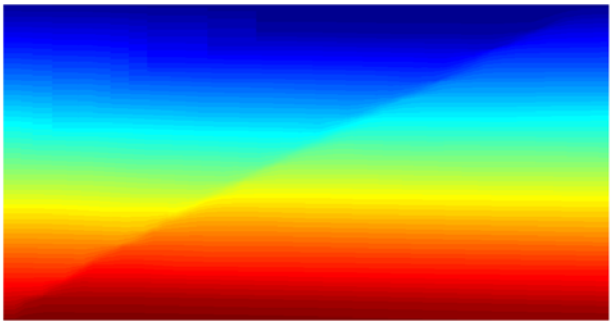

Fig. 7a $\Delta\varphi_D$ for the Doppler picture

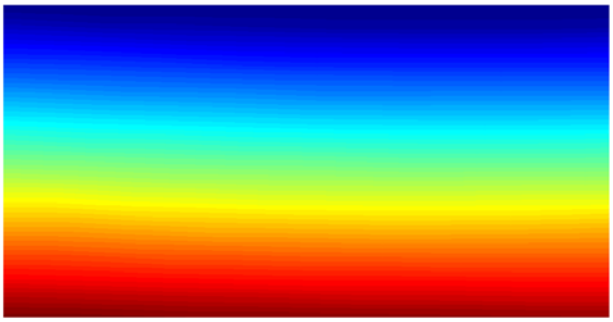

Fig. 7b φ_R for the reference picture

Further on, according to equation (4), both phase differences, $\Delta\varphi_R$ and $\Delta\varphi_D$ are subtracted from each other at every point of the $n \times m$ matrix: $\Delta\varphi_D - \Delta\varphi_R = d(\Delta\varphi)$. Inserting $d(\Delta\varphi)$ into equation (4), the frequency shift $d\nu$ is obtained at all grid points, representing in the object plane Σ the light sheet plane coordinates x and y. For calculating the value of the tracer velocity v the following relation, using the angles γ_1 and γ_2 as explained in Fig. 4, is applied:

$$|v| = \frac{d\nu}{\nu_L} \frac{c}{(\cos\gamma_1 + \cos\gamma_2)} \,. \tag{8}$$

4.3 Velocity outcomes

The image processing algorithm deals with the arrangement of the vertical velocity v appearing in the light sheet plane illuminating the wedge flow. The velocity picture of Fig. 8 shows in pseudo colours at the $n \times m$ mesh points the visualized formation of the vertical v velocity present in the

free stream flow and behind the oblique attached shock wave over the wedge surface. The flow produced by the Mach-6-nozzle is quite parallel with almost no vertical v-component, i.e., $v = 0 \pm 25$ m/s, see blue zone in Fig. 8. On the wedge, the measured velocity is of the order of $v = 525$ m/s $\pm$ 25 m/s, as visualized in red in the velocity picture of Fig. 8 being constant between bow wave and wedge surface. The total measuring error for the processing tools applied is estimated to be about $\pm$ 25 m/s. The particle inertia causes the bow wave velocity jump to be smeared over a thickness of 2 mm to accelerate the tracer particles from $v = 0$ in front of the bow wave to the vertical flow velocity $v = 525$ m/s, present over the wedge surface. The deviation between the calculated v-velocity of 546 m/s and the measured one is within the measuring error, showing that DPV is suitable for visualizing absolute tracer velocities.

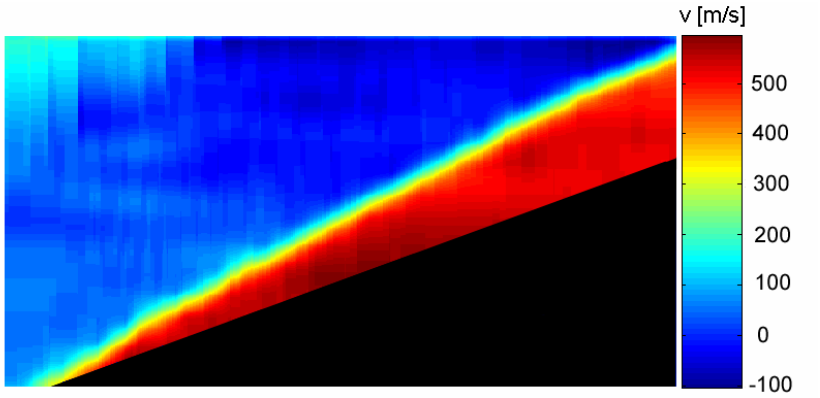

Fig. 8 DPV velocity distribution over the wedge visualized in pseudo colours

The vertical velocity distribution for a sphere is represented in Fig. 9. In contrast to the wedge flow Doppler picture in Fig. 8, which has been illuminated 2 ms by an Ar^+-laser, here a pulsed Nd-YAG-laser was used with a 40 ns pulse width and 532 nm wavelength. The energy output was 180 mJ. The separation of reference and Doppler pictures was well achieved using the longer extended Ar^+-laser light. With the short duration Nd-YAG laser light pulse separation of reference and Doppler picture was not completely reached as using the longer extended Ar^+-laser light so that further research will be necessary.

At the centre line in front of the sphere (Fig. 9), the v-velocity component is expected to be zero as it is in the flow coming out of the contoured nozzle. This is very well reproduced by the DPV method, see pseudo colour scale in Fig. 9. Over the sphere, the flow accelerates to slightly more than 500 m/s. A Doppler picture for a flow around a cylinder is shown in Seiler et al.(2008b).

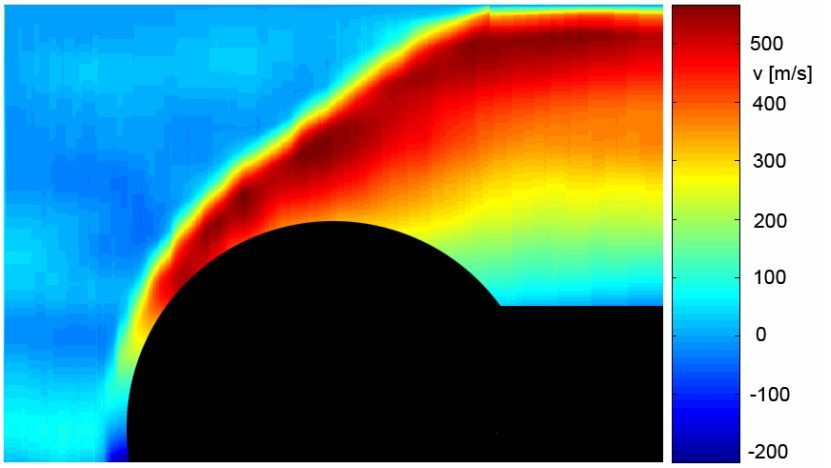

Fig. 9 DPV velocity distribution around a sphere

5 Automated FFT technique

5.1 Requirements

In order to measure the fringe displacements automatically, the Doppler pictures must fulfil the following requirements:

1. The maximum fringe shift (measured in pixels) should not exceed half of the distance between the minima of two fringes ($\Delta\varphi \leq \pi$), i.e., the fringe spacing. Therefore, the glass block used in the MI has to be adapted to the expected velocity range.
2. Reference and Doppler images need to be matched in size and rotation. Marker images should be taken before the experiment.

5.2 Image filtering

The captured Doppler images contain the velocity variation information in form of fringe displacements. The original MI in Mach-6-flow taken reference and Doppler images are given in Fig. 10 with the fringe arrangement obviously present in both pictures. In the flow in front of the oblique shock produced over the wedge surface the vertical velocity is zero, i.e. there the initially tuned fringe pattern is present as it is in the reference sample. By the oblique shock, the flow turns upwards and the fringes are shifted as seen in the Doppler picture in Fig. 10. The Doppler images are filtered first to facilitate the automated detection of fringe shifts by the computer. All unwanted brightness variations not belonging to the fringe system and high-frequency background noise are removed from the pictures while preserving the original fringe displacements in all details. Fig. 11 shows the filtered reference and Doppler pictures for the flow over the wedge from Fig. 10.

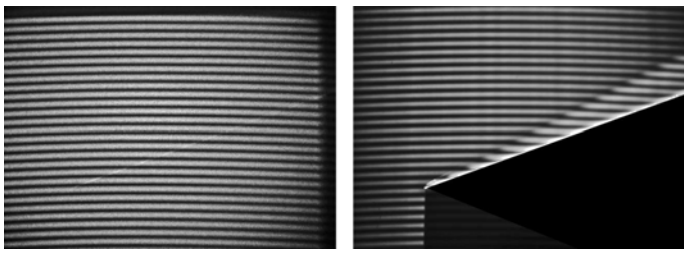

Fig. 10 Original reference and Doppler pictures

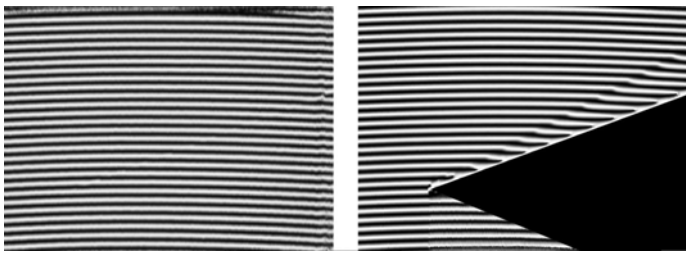

Fig. 11 Filtered reference and Doppler pictures

5.3 Velocity profile calculation

An automated DPV algorithm then processes the filtered images. Additionally, two black/white mask images are needed, one masking out non-analyzable areas (e.g. saturations, no tracers) and one image masking out the model contour to show its placement in the shock-tunnel and its

dimensions. Equation (9) describes the brightness information of each pixel of the filtered Doppler image as:

$$g(x,y)=c(x,y)e^{j2\pi f_0 y}+c^*(x,y)e^{-j2\pi f_0 y}. \quad (9)$$

A value of g(x, y) = -1 corresponds to the brightness minimum, a value of g(x, y) = 1 to the maximum and the parameter j is $\sqrt{-1}$. The phase shift can be found in c(x, y) or its complex conjugate c*(x, y):

$$c(x,y)=\frac{1}{2}b(x,y)e^{j\Delta\varphi(x,y)}. \quad (10)$$

To extract the phase shift information from equation (10), each column of the Doppler image is transformed in the frequency domain using the FFT:

$$G(f,x)=C(f-f_0,x)+C^*(f-f_0,x). \quad (11)$$

An example column of a typical Doppler image is seen in Fig. 12.

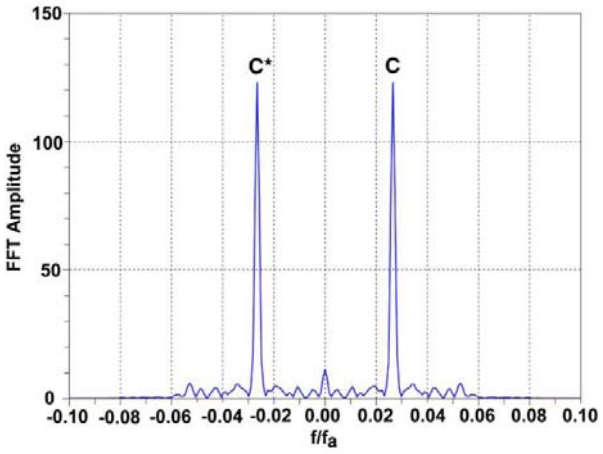

Fig. 12 FFT of an example column of a typical Doppler image

In the next step the sideband C is left shifted on the frequency axis by f_0 to get the spectrum C containing the phase difference information in the base band (demodulation). To obtain the distribution of the phase difference Δφ(x, y) the spectrum is transformed back from frequency domain C(x, y) to the image domain c(x, y) using the Inverse Fast Fourier Transformation (IFFT). Finally, the complex logarithm of c(x, y) is calculated as follows:

$$\ln[c(x,y)]=\ln\left[\frac{1}{2}b(x,y)\right]+j\,\Delta\varphi(x,y). \quad (12)$$

The phase difference Δφ(x, y) is now completely separated from any amplitude variation in the imaginary part of equation (12). Applying the operations described pixel by pixel to all image columns of the reference and Doppler pictures, the change of the phase differences between both is as:

$$d(\Delta\varphi)(x,y)=\Delta\varphi_D(x,y)-\Delta\varphi_R(x,y). \quad (13)$$

The phase difference variations are proportional to the velocity variation dv:

$$dv(x,y)=v(x,y)=\frac{A}{2\pi}d(\Delta\varphi)(x,y). \quad (14)$$

The value of the proportionality factor A in equation (14) depends on the length of the glass block used in the Michelson interferometer and the wavelength of the laser used. With the reference image being defined as zero velocity the absolute velocity v(x, y) is equal to the velocity variation dv(x, y).

5.4 FFT velocity results

The velocity picture in Fig. 13 shows in pseudo colours the vertical velocity component *v* present in both the free stream flow and behind the oblique attached shock wave placed in front of the wedge. On the wedge, the measured velocity is of the order of $v \approx 550 \pm 25$ m/s, as visualized in orange in the velocity picture, being constant between bow wave and wedge surface.

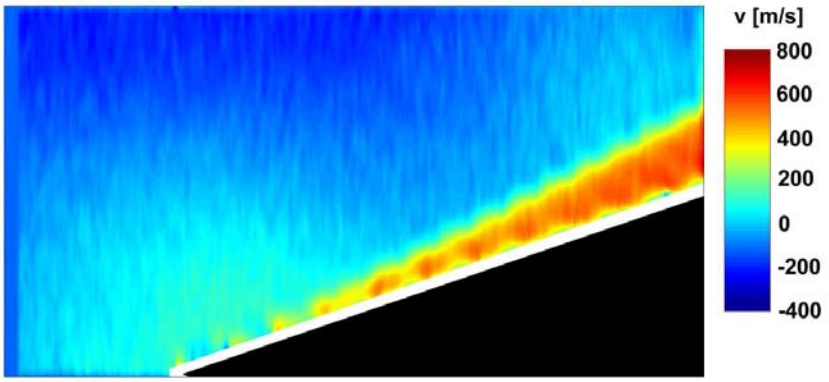

Fig. 13 FFT processed velocity distribution over the wedge

The vertical velocity distribution for a sphere is represented in Fig. 14. Over the sphere, the flow accelerates to slightly more than 500 ± 25 m/s. The results of the sphere as well as the wedge velocity measurements are, regarding a measuring error of about ± 25 m/s, in good agreement with numerical estimations.

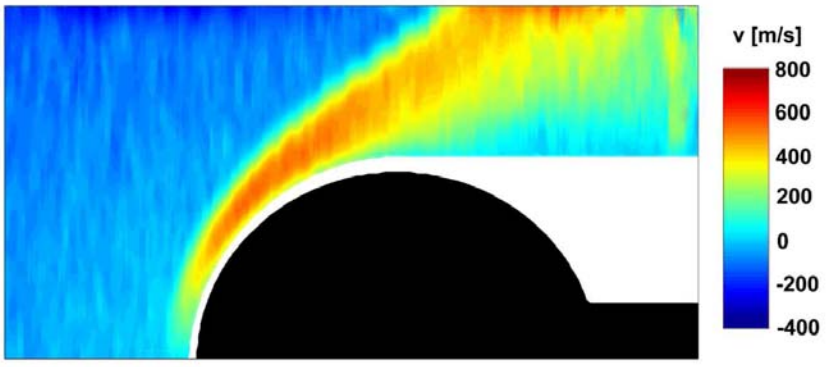

Fig. 14 FFT processed velocity distribution around a sphere

6 Conclusions

The motivation for the authors to further develop and improve the DPV-technique, especially the processing algorithms, is found in future applications for visualizing and measuring velocities in hypersonic flows up to several kilometres per second, typical of re-entry conditions. The velocity

range for the DPV technique is theoretically limited only by the speed of light, whereas with PIV the maximum measured velocities are in the range of 2 km/s. Especially this PIV restriction motivated the authors to further develop the DPV technique for these measurements.

The optics for taking DPV pictures in the MI-system were improved to further optimize the separation of the simultaneously illuminated Doppler and reference pictures as well as to reduce the unwanted speckle noise in the reference image. The presented semi-automated method is especially convenient when the requirements discussed in 5.1 cannot be fulfilled. Otherwise, the automated FFT algorithm is less time consuming and therefore the preferred one. The DPV technique using these tools was tested by taking Doppler pictures of the flow around a wedge and a sphere in a Mach-6-nozzle flow. The measured and visualized velocity distributions agree very well with theoretical estimations, numerical calculations using CFD++ and PIV measurements by Havermann et al. (2002).

References

Havermann M, Haertig J, Rey C, George A (2002) Application of Particle image velocimetry to high-speed supersonic flows in a shock tunnel. In: Proceedings of the 11th International Symposium on Applications of Laser Techniques to Fluid Mechanics, Lisbon, Portugal

Merzkirch W (1990) Laser-Speckle-Velocimetrie. „Lasermethoden in der Strömungsmechanik“. Hrsg. Ruck B., AT-Fachverlag, Stuttgart

Meyers JF (1992) Doppler Global Velocimetry the next generation. AIAA 92-3897

Oertel H, Seiler F, George A (1982) Visualisierung von Geschwindigkeitsfeldern mit Dopplerbildern. (Visualization of velocity fields with Doppler pictures). ISL-Report R 115/82

Pichler A, George A, Seiler F, Srulijes J, Havermann M (2007) Doppler Picture Velocimetry (PDV) applied to hypersonics. In: Proceedings of the 26th Int. Symposium on Shock Waves, Göttingen, Germany

Pfaff R, George A, Seiler F, Srulijes J (2005) Dopplerbild-Verfahren-Entwicklung einer neuen Auswertemethode. ISL-Report R 124

Pfaff R (2007) Automated processing of the ISL Doppler images. Bachelor thesis, Fern Universität Hagen

Pfaff R, Pichler A, George A, Seiler F (2007) Model based image processing for flow visualisation. In: Proceedings of International Conference on Systems Science, Wroclaw, Poland

Seiler F, Srulijes J, George A (1987) A Doppler-picture camera for velocity field visualization. In: Proceedings of the 12th Int. Congress on Instrumentation in Aerospace Simulation Facilities, Williamsburg, USA

Seiler F, George A, Leopold F, Havermann M, Srulijes J (2002) Enhanced Doppler Picture Velocimetry (DPV) for planar velocity measurements in high speed shock tunnel flow. In: Proceedings of the 10th Int. Symposium on Flow Visualization, Kyoto, Japan

Seiler F, George A, Havermann M, Srulijes J (2004) Doppler Picture Velocimetry (DPV) applied to high-speed shock tunnel flows. In: Proceedings of the 11th Int. Symposium on Flow Visualization, Notre Dame, Indiana, USA

Seiler F, George A, Srulijes J, Havermann M (2006) Progress in Doppler Picture Velocimetry (DPV) Technique. In: Proceedings of the 12th International Symposium on Flow Visualization, Göttingen, Germany

Seiler F, Pichler A, Pfaff R, Srulijes J (2008a) Novel Automated Doppler Picture Velocimetry (DPV) Processing Tools. In: Proceedings of the 13th International Symposium on Flow Visualization (ISFV13), Nice, France

Seiler F, George A, Srulijes J, Havermann M (2008b) Progress in Doppler picture Velocimetry (DPV). Exp Fluid 44:389-395

Sun Microsystems Inc. (2005), What is Java Advanced Imaging? java.sun.com/products/java-media/jai/whatis.html

The MathWorks Inc., Image Processing (2005) Link to: www.mathworks.com/applications/imageprocessing/description/ analysis.html